Tunable Morphology of Polyaniline/Multi-wall Carbon Nanotube for Organic Solar Cells

Zeinab Jarrahi [a], Golamali Farzi [a,*], Reza Charekhah [a], Mahsa Darabi [a], Alexis Fisher [b]

[a] *Department of Polymer Engineering, Faculty of Petroleum and Petrochemical Engineering, Hakim Sabzevari University, P. O. Box 397, Sabzevar, Iran*

[b] *Laboratoire de Physique des Lasers, Université Sorbonne Paris Nord, CNRS, (UMR 7538), 99 av. JB Clément, 93450 Villetaneuse, France*

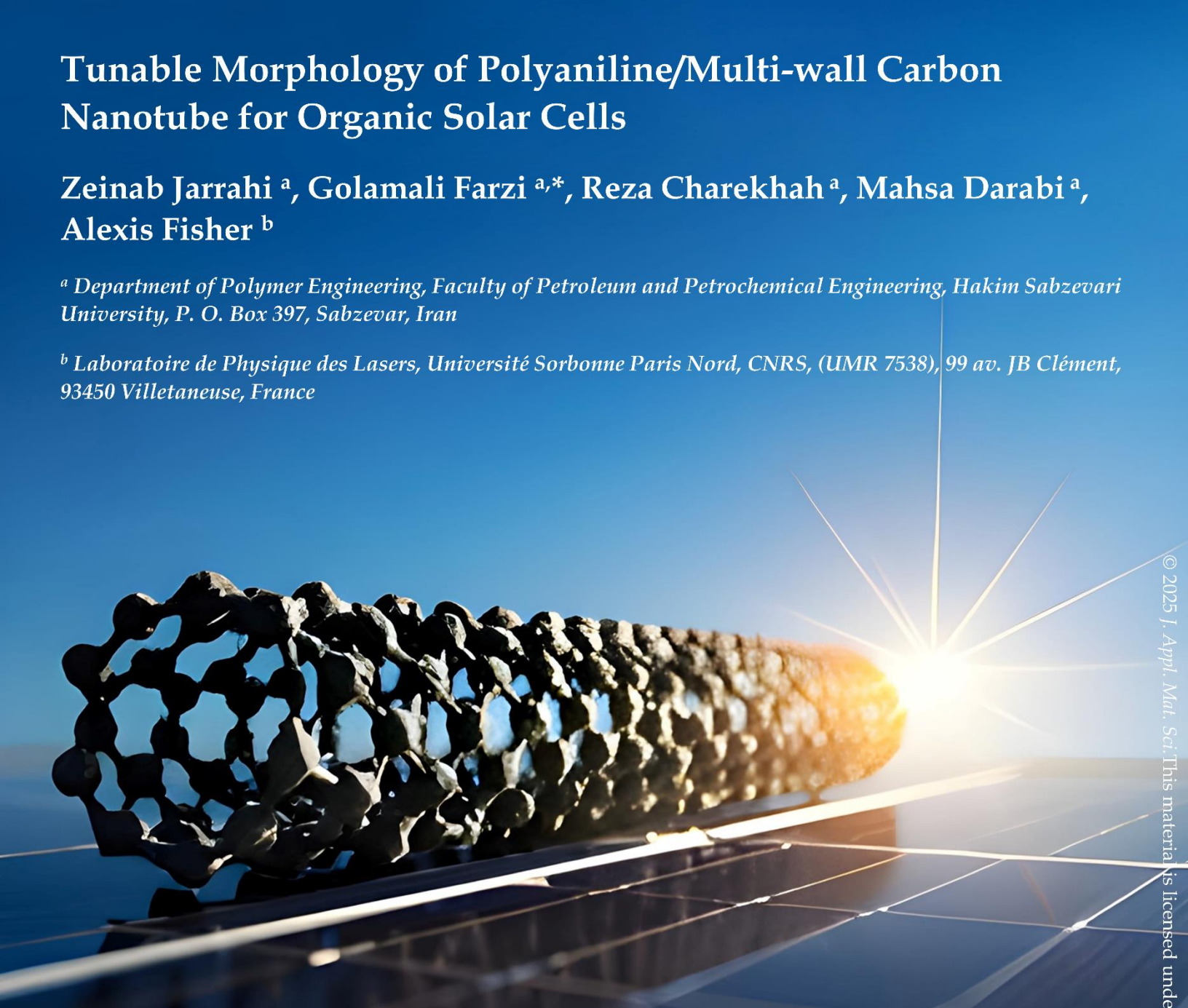

Editor's note: The main factors that limit the power conversion efficiency of organic solar cells are exciton dissociation, charge transport, and charge recombination. Jarrahi et al. proposed enhancing the efficiency of polyaniline-based organic solar cells by controlling their morphology through the incorporation of multi-walled carbon nanotubes and adjusting the polymerization conditions.

doi: 10.22034/jams.2024.210130

How to cite: Z. Jarrahi et al. *Journal of Applied Material Science*, **2025**, *1*, 210130.

JOURNAL OF
APPLIED
MATERIAL
SCIENCE
jams.hsu.ac.ir

Journal of Applied Material Science **2025**, *1*, 210130
How to cite: Z. Jarrahi et al., *Journal of Applied Material Science*, **2025**, *1*, 210130.
Journal homepage: **www.jams.hsu.ac.ir**

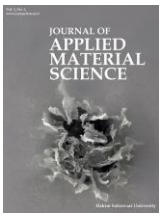

Original Research

Tunable Morphology of Polyaniline/Multi-wall Carbon Nanotube for Organic Solar Cells

Zeinab Jarrahi [a], Golamali Farzi [a,*], Reza Charekhah [a], Mahsa Darabi [a], Alexis Fisher [b]

[a] *Department of Polymer Engineering, Faculty of Petroleum and Petrochemical Engineering, Hakim Sabzevari University, P. O. Box 397, Sabzevar, Iran*

[b] *Laboratoire de Physique des Lasers, Université Sorbonne Paris Nord, CNRS, (UMR 7538), 99 av. JB Clément, 93450 Villetaneuse, France*

Abstract

Despite the great interest in applying polyaniline (PAni) in organic solar cells (OSCs), only a few studies deal with the morphology control of PAni-based OSCs. Here, comprehensive research has been conducted on the morphology control of PAni/multi-walled carbon nanotubes (MWCNTs) nanocomposites. Our results show that the morphology of PAni/MWCNTs can be tuned to tubular or cauliflower by controlling the synthesis parameters. The present study discusses the effect of the dopant's nature, the process's temperature, and the polymerization kinetics on the morphological dominance in the structure of PAni/MWCNTs nanocomposites. Also, the impact of the morphology of PAni/MWCNT on the efficiency of Photovoltaic cells based on these nanocomposites is investigated using Fourier transform-infrared spectroscopy, Hall effect measurements, UV-visible analyses for band gap measurements, and field emission scanning electron microscopy. The results revealed that by controlling morphology and achieving the desired morphology (tubular morphology), the conductivity of nanocomposite and mobility of the charge carriers increases. Consequently, it has been shown that the efficiency of PAni/MWCNTs OSCs increases due to the beneficial changes in short circuit current density, open voltage, and Fill Factor. Our results concluded that morphology control in synthesizing PAni/MWCNT nanocomposites plays a crucial role in the efficiency adjustment of the resultant photovoltaic devices.

Keywords: Polymer nanocomposites; Organic solar cells; Morphology control; Band gap.

1. Introduction

In recent decades, OSCs have garnered significant interest from researchers due to their lightweight nature, flexibility, cost-effective raw materials, and ease of processing. However, OSCs are challenged mostly due to their low efficiency [1-4]. The bottlenecks that limit the progress of power conversion efficiency for OSCs are exciton dissociation, charge transport, and charge recombination. [5-7] Hence, various approaches have

* Corresponding author.
Email addresses: farzi@hsu.ac.ir (G. Farzi)

Received 7 November 2024
Revised 18 December 2024
Accepted 25 December 2024
Available online 28 December 2024

https://doi.org/10.22034/jams.2024.210130

attempted to improve these shortcomings [5, 8]. One strategy to accomplish this aim is incorporating carbon nanotubes (CNTs) into conducting polymers [9-14].

Conducting polymer/CNTs nanocomposites are a class of materials increasingly used in optical and electrical applications, particularly in polymer solar cells [15]. Effective utilization of CNTs for fabricating nanocomposites relies on the uniform dispersion of CNTs within the conductive polymer matrix. This uniformity optimizes the interfacial area for charge transfer between the CNTs and matrix [16, 17]. One effective method to achieve intimate dispersion of CNTs in a polymer matrix is in-situ polymerization [18].

Many polymers, such as polypyrrole, polyaniline (PAni), etc., have been used as matrix materials in these nanocomposites. Among these, polyaniline has been greatly considered due to the low cost and availability of raw materials, easy synthesis, relatively good environmental stability, high electrical conductivity, and simple doping/dedoping chemistry [19-25]. Polyaniline in emeraldine salt (ES) is synthesized through the oxidative polymerization of aniline using a chemical oxidant such as ammonium persulfate (APS) or ferric chloride (3FeCl), or via electrochemical oxidation in an acidic environment [25, 26].

Figure 1 illustrates the structure of each of the units of PAni, benzenoid diamine/quinoid diamine units, which are based on the reduction or the oxidation state. The formation of a charge-transfer complex between CNTs and polyaniline was demonstrated by the appearance of new absorption in the visible region [27]. Also, the observed enhanced conductivity effect was related to the fact that CNTs might serve as a conducting bridge between the PAni ES domains due to their large aspect ratio and surface area [28, 29].

Much research has been carried out on the conductivity of polyaniline/CNTs nanocomposites [28, 30]; however, to the best of our knowledge, there is no comprehensive investigation on the morphology control of these nanocomposites. The nanomorphology of BHJ blend films is at the center of the charge transfer process [31-33]. Controlling the nanomorphology in the active layer would improve the photocurrent conversion along with the FF [34] because efficient excitonic dissociation and charge transfer strongly depend on the fine morphology of the active layer [35, 36]. However, such performance can be improved when combined with device engineering.

Here, a comprehensive morphological study provides insight into different PAni/MWCNTs nanocomposite morphologies, including cauliflower (reported in our previous work [37]) and tubular. This was carried out by controlling several parameters influencing the aniline polymerization process. Then, in the next step, the active layer of the solar cell was fabricated based on polyaniline/MWCNTs nanocomposites, and the impact of the tuned morphology on the solar cell efficiency was understood. The physical and electrical properties of the two types of morphologies and their solar cells were comparatively investigated for a more in-depth insight. It was found that straw change in the synthesis parameters resulted in significant improvement of morphology and, consequently, the performance of the solar cell.

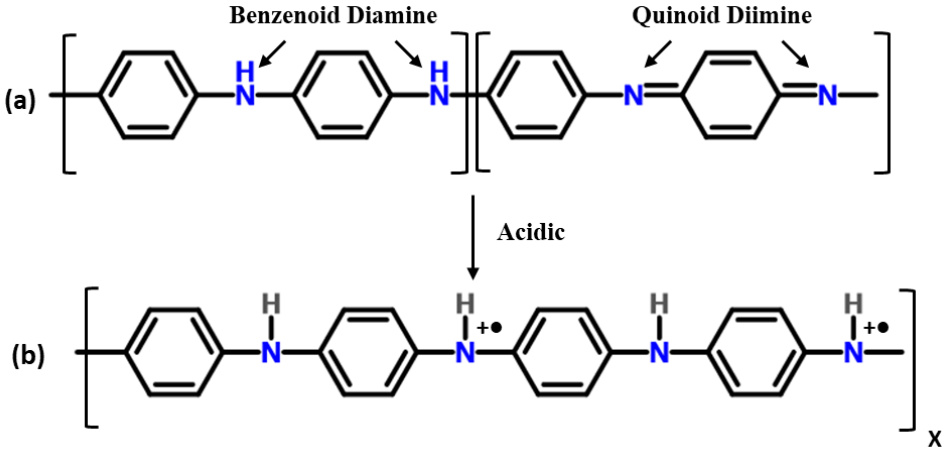

Figure 1. (a) Chemical structure of the undoped polyaniline (emeraldine base) and (b) its doped form (emeraldine base salt)

2. Experimental

2.1. Materials

Aniline monomer (purchased from Merck), MWCNTs (multi-walled carbon nanotubes, with 20–30 nm diameter, 20 µm length, and density 2.1 g/cm³, purchased from Sigma-Aldrich), ammonium peroxydisulfate (APS, purchased from Merck), and p-toluene sulfonic acid (p-TSA, purchased from Sigma-Aldrich) were used as the starting materials. Several PAni/MWCNT nanocomposites were synthesized with varying MWCNTs weight percentages ranging from 0% to 10%. The two types of morphology, cauliflower and tubular, were obtained by controlling synthesis parameters such as temperature, ultrasonic duration, and reaction and polymerization rates. Multi-layer OSCs were fabricated using PAni/MWCNTs nanocomposites with different weight percentages of MWCNT. The detailed procedure for nanocomposite synthesis and solar cell fabrication has been reported in our previous work [37].

2.2. Measurements

FTIR (Fourier Transform Infrared Spectroscopy, PerkinElmer Spectrum Two) was utilized to identify the functional groups and chemical bonding within the nanocomposites, while UV-Visible Spectroscopy (Shimadzu UV-2600) provided insights into their optical absorption properties. Atomic Force Microscopy (AFM, Bruker Dimension Icon) was employed to study the surface morphology and roughness, and Thermal Gravimetric Analysis (TGA, TA Instruments Q500) was used to assess the thermal stability and decomposition behavior. Scanning Electron Microscopy (SEM, JEOL JSM-7610F) offered detailed morphological analysis to confirm the formation of nanostructures, and the Hall Effect technique (Keithley 2400) was applied to measure carrier concentration and mobility. Then, the photovoltaic and electrical properties of the fabricated solar cells were characterized by a I-V tracer (Sharif Solar IV-28) under the illumination of AM 1.5, 100 $mWcm^{-2}$.

3. Results and discussion

3.1. Synthesis and morphology control of tubular PAni/MWCNT nanocomposite

This section investigated the effects of synthesis parameters (the dopant's nature, the synthesis kinetics, and the synthesis temperature) on morphology control of PAni/MWCNT nanocomposites. Then, the band gap of the nanocomposites with either morphology (cauliflower / tubular morphologies) was compared.

Polyaniline (emeraldine base) is essentially different in some aspects, such as its behavior with other conjugated polymers [38]. Firstly, its structure is not conjugate and symmetric, so the energy band gap and Fermi level do not form in the center of the π-bond, so its conduction band and valence band are irregular. Its energy level position after dope differs from regular conjugated polymers, such as polyacetylene or polythiophene. Secondly, the carbon ring and nitrogen atoms are in their conjugate length and a polymer with an A-B structure; this is in contrast with that of polypyrrole or polythiophene, in which the non-main chain atoms are formed while they do not participate much in the formation of the π-bond. Thirdly, the emeraldine base can be converted from non-conductive to metal-like conductive by proton absorption in places N=, while the number of electrons is constant.

Figure 1 indicates an emeraldine base with an acid. The emeraldine salt state can form whose metallic features will be represented by creating a polar network in the structure. This feature will give rise to new optical and structural characteristics like the material. However, partial protonation can cause separation between protonated and non-protonated sites in the structure.

3.1.1. Nature of the dopant

The movement of electrons within the π-framework is the source of conductivity. However, a dopant is required to increase the level of conductivity for these nanocomposites [26]. In synthesizing PAni/MWCNT nanocomposite, suitable dopants for the cauliflower and tubular morphology are *p*-toluene sulfonic acid (*p*-TSA) and hydrochloric acid (HCl), respectively [37]. The process of HCl doping requires sodium dodecyl sulfate (SDS) to improve the dispersion of the carbon nanotubes in the polymer matrix. As seen in the map of electrostatic potential (MEP) in Figure 2, *p*-TSA acts with more surface dipole as a surfactant and does not require surface active materials, such as SDS, during its synthesis [39].

Because of the relatively high polarization of its molecules and, therefore, high attraction of its molecules to one another, non-doped polyaniline has low solubility, especially in non-polar solvents. This Van der

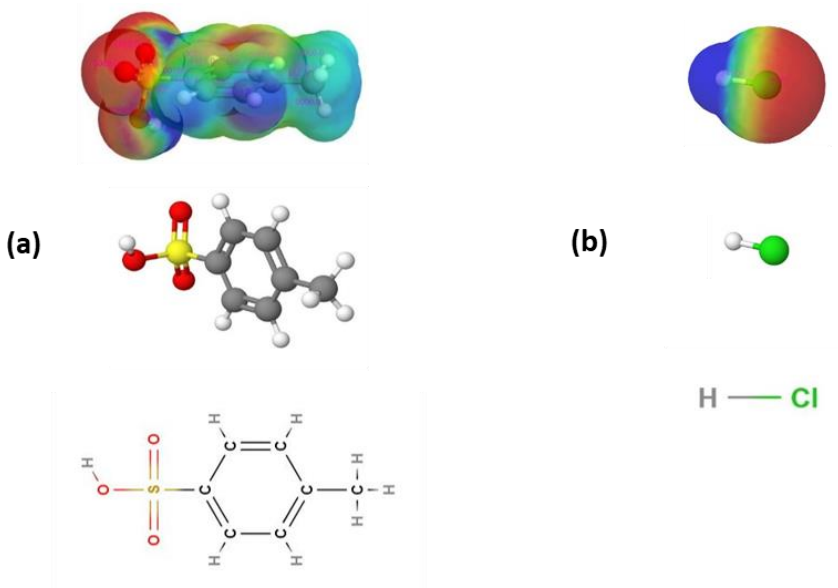

Figure 2. Molecular structure and MEP of (a) p-TSA and (b) HCl

Waals force between polyaniline molecules is such that even with its strong conventional polar solvents such as dimethylformamide (DMF) and N-methyl-2-pyrrolidone (NMP), non-doped polyaniline is not well solved and doped polyaniline has better solubility due to polarization changes and intermolecular force reduction [39].

In this context, a dopant such as *p*-TSA with a larger chain length than a small molecule such as HCl further reduces the polyaniline polarization, making it solvable more effectively by creating a greater gap between the molecules as a steric stabilizer agent. As shown in Figure 3, by increasing solubility, the separation of polyaniline chains in the synthesis environment increases, and the

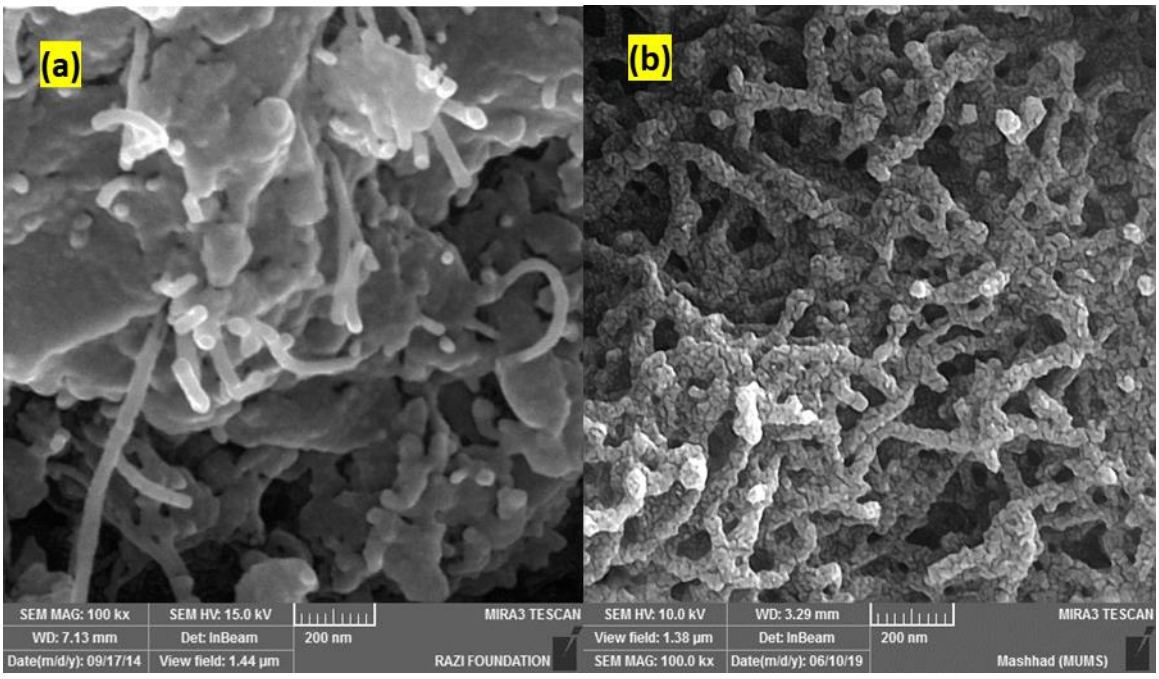

Figure 3. FESEM images of 10% MWCNTs/PAni: (a) cauliflower morphology by using HCl and (b) tubular morphology by using *p*-TSA.

formation of large polyaniline masses (polyaniline coagulations) is reduced around the carbon nanotubes and, more specifically, on their surface. Therefore, the PAni/MWCNTs nanocomposite morphology changes from cauliflower to tubular, so that physical and photovoltaic properties are affected.

It was noted that polyaniline produced by doping with HCl had a higher conductivity than that produced by doping with *p*-TSA. The results obtained in a previous work by our group confirmed this issue, [37]. However, in the present study, after the synthesis of nanocomposites composed of CNTs and polyaniline, the results were reversed, and the conductivity of the nanocomposite produced by polyaniline doped with *p*-TSA was higher than HCl doped nanocomposite. The reason for this behavioral rotation could be that, in addition to the effect on the conductivity of polyaniline (due to the change of charge distribution in the aniline molecule and the effect on the movement of electrons in the length of conjugate bonds), the dopant also affected the morphology of the PAni/MWCNT nanocomposites and this could be due to the change in the interaction between polyaniline and nanotubes (depending on the nature of dopant and reaction condition). Therefore, although the use of *p*-TSA reduced the conductivity of pure polyaniline rather than the use of HCl, the resulting nanocomposite led to more electrons reaching into the preferred paths of carbon nanotubes due to the tubular morphology of low-amount polyaniline on the surface of the nanotubes, as shown in Figure 3b; thus, conductivity was higher than the doped nanocomposite with HCl due to the cauliflower morphology with high polyaniline thicknesses (greater domain size) and long paths for the electrons to reach the carbon nanotubes [40, 41]. In addition, increasing order in the polymer structure, more homogeneity, and the emergence of tubular morphology also increased the mobility of charge carriers [36].

Table 1 summarized the conductivity and electron mobility of nanocomposites with two morphologies achieved by Hall Effect measurement. As reported in this table, higher conductivity of the PAni/MWCNTs nanocomposite synthesized via *p*-TSA suggests that this nanocomposite is a better option for being used as the active layer leading to the improvement of photovoltaic characteristics due to tubular morphology (discussed below), increased solubility, as well as increased film formation ability, all of which are important parameters for fabricating solar cells.

The interaction between PAni and carbon nanotubes with different dopants can be investigated by examining the activity of the corresponding chemical bonds. Figure 4 shows the FTIR spectra of pure polyaniline (emeraldine salt), a cauliflower morphology 10% nanocomposite (doped by HCl), and a tubular morphology 10% nanocomposite (doped by *p*-TSA). As shown in Figure 4, peaks in the range 2897 cm^{-1} correspond to the S-O and C-H stretching in the benzenoid ring, peaks 551 and 657 cm^{-1} correspond to the C-H stretching vibrations, and also the presence of peaks 1044 of the $(SO_3)^-$ functional group, the peak of 750 cm^{-1} (stretching S-O) and the peak of 630 cm^{-1} (stretching C-S), which are related to the connection of $(SO_3)^-$ functional groups to the polyaniline aromatic rings confirm the presence of *p*-TSA in the nanocomposite (blue spectrum) in comparison with other spectra.

Also, the non-removal and maintenance of the ratio of quinoid and benzenoid peaks (1466 and 1559 cm^{-1}) representing polyaniline demonstrate π-interaction between the aromatic aniline and nanotube components and aniline absorption on the surface of the nanotubes in the nanocomposites (red and blue spectra). The wider peaks in this range indicate increased vibrational activity in their structure, and reducing the difference between quinoid and benzenoid peaks (i.e., increasing the intensity of quinoid peak) is due to the π-bonding of the carbon nanotube with the π-conjugated structure of polyaniline, particularly in quinoid units.

Peaks from 1125 cm^{-1} to 1148 cm^{-1} relate to the C-H plate bending vibrations formed during the polyaniline

Table 1. Conductivity and solubility of polyaniline synthesized with HCl and p-TSA in DMF, as well as conductivity and charge carrier of nanocomposites with two morphologies

Characteristic	PAni-HCl	Pani-*p*-TSA	Pani-HCl/MWCNTs (Cauliflower morphology)	Pani-*p*-TSA/MWCNTs (Tubular morphology)
Conductivity (S/cm)	3.32	2.11	3.6	3.95
Solubility at 25 °C (g/L)	4	9	4.5	8
Solubility at 5 °C (g/L)	1	3	0.8	2.1
Electron mobility ($cm^2/V.s$)	-	-	4.46×10^{-6}	5.48×10^{-4}

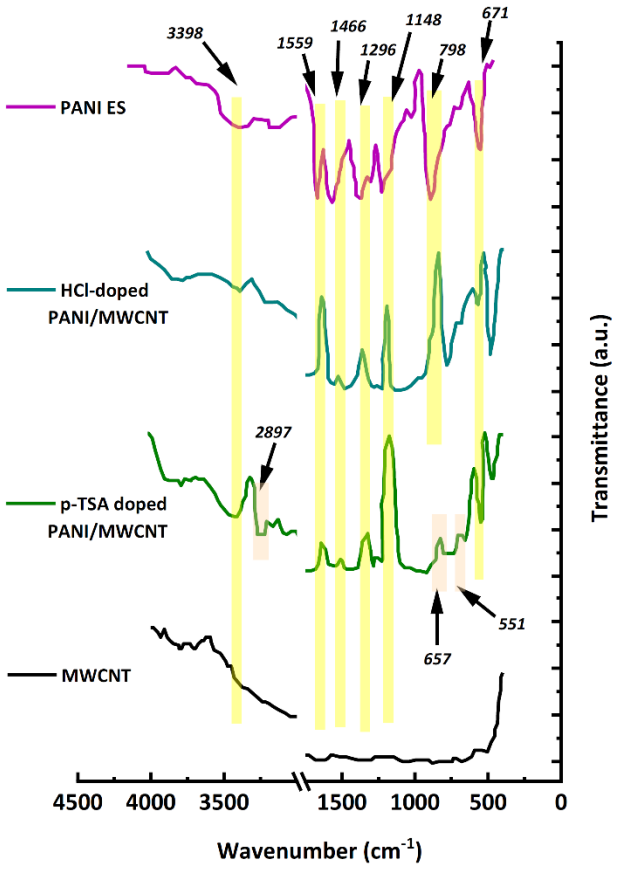

Figure 4. FTIR spectra of emeraldine salt, PAni/MWCNTs doped with HCl, PAni/MWCNTs doped with *p*-TSA, and MWCNTs.

chain's protonation. These peaks represent the non-localized state of electrical charges. As seen in this figure, in this range, the spectrum of doped nanocomposite with *p*-TSA is wider and shifted to fewer frequencies. This is due to the change like the anion produced by *p*-TSA $(SO_3)^-$ relative to HCl (Cl^-), which subsequently results in a change in the C-H plate bending and N-H stretching frequency variation and, as a result, in the different distribution of charge in the quinoid ring. This difference in the charge distribution of the quinoid ring reduces the conductivity of the polyaniline doped with *p*-TSA relative to the HCl-doped polyaniline.

N-H stretching vibrations are observed at 3354 – 3398 cm^{-1}. The intensity of this peak in the HCl-doped PAni/MWCNTs is greater than that of pure polyaniline and is the highest in *p*-TSA-doped PAni/MWCNTs. The sharpening of this peak represents a better transfer of proton from polyaniline to the carbon nanotube network and a better substitution of hydrogen atoms in the amine group. The carbon atom of carbon nanotubes competes with polyaniline nitrogen in absorbing anion. According to the MEP (map of electrostatic potential) of the two dopants (Figure 2), the absorption of $(SO_3)^-$ by the nanotubes is more than Cl^-, resulting in better adhesion of the polyaniline doped with *p*-TSA to the nanotube surface, which represent tubular morphology.

3.1.2. Sonication time

Before polymerization, a mixture of carbon nanotubes and aniline monomers is placed under ultrasonic conditions in aqueous media. The longer sonication time results in better homogenous dispersion of the nanotubes in the mixture of water and aniline, and consequently, the coagulation of MWCNTs is avoided.

3.1.3. Kinetics of the synthesis

In the previous stage, carbon nanotubes were well dispersed between aniline monomers, so many aniline molecules surrounded each nanotube. The rate of addition of the dopant and initiator blended to the

reactor containing the mixture of carbon nanotubes and aniline monomers played a decisive role in the polymerization stage. The lower the addition rate, the more dopant and initiator molecules could join the aniline monomers on the surface of carbon nanotubes and prevent coagulation of polyaniline chains and phase separation. During this long period, initiator radicals could attack more aniline molecules located on the surface of the carbon nanotubes and begin the heterogeneous nucleation from the surface of the MWCNTs. Therefore, much of the carbon nanotube surface was covered with polyaniline chains, as shown in Figure 5a; thus, tubular morphology became predominant. Conversely, if the droplets were added more quickly, instead of attacking the aniline molecules on the surface of the MWCNTs, initiator radicals intended to attack the scattered available aniline molecules in the synthesis environment. Thus, as in

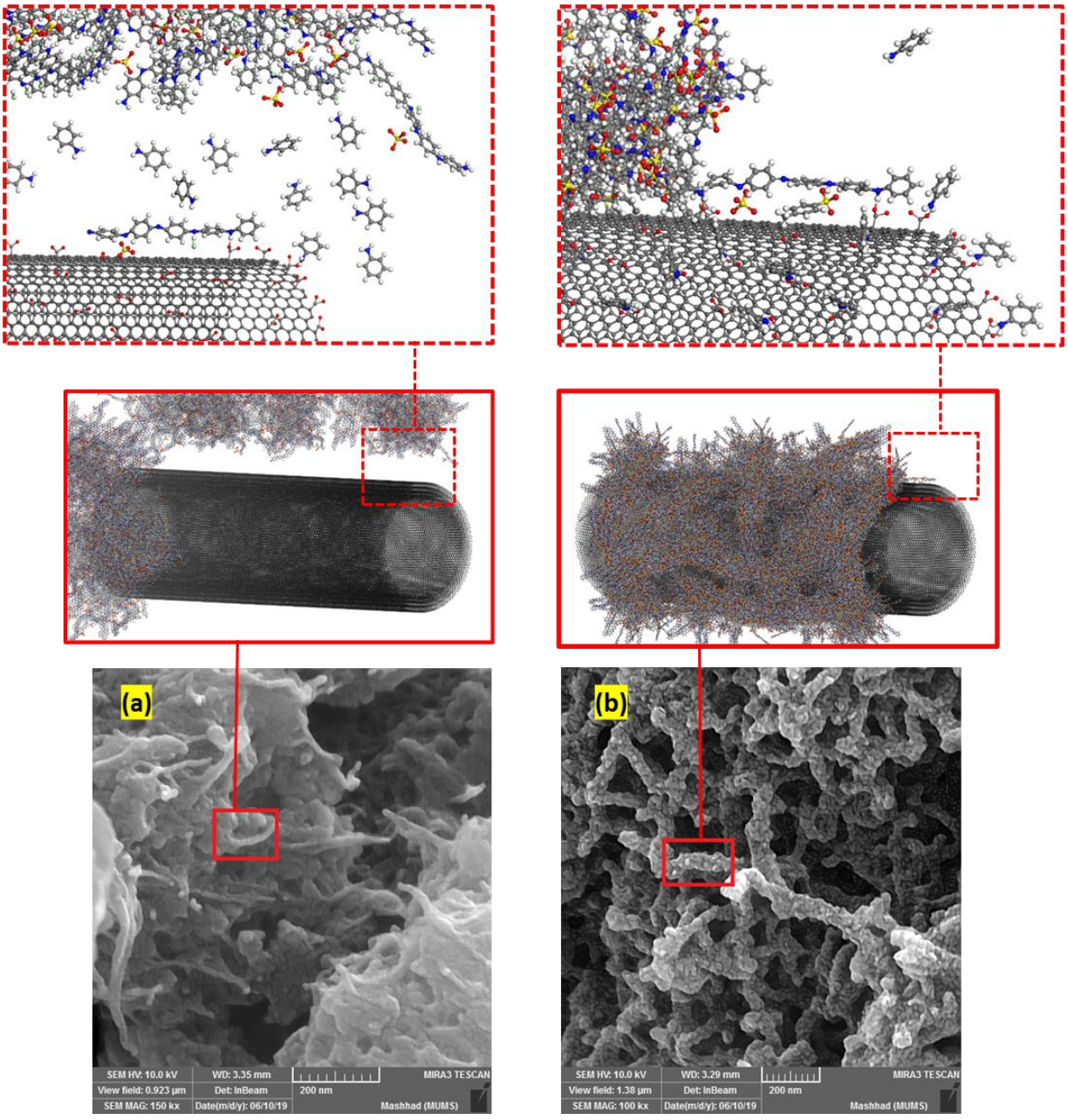

Figure 5. (a) Imperfect and (b) full function of the initiator and dopant in the aniline polymerization on the surface of 10% MWCNTs.

Figure 5b, polymerization often occurred through homogeneous nucleation, and the cauliflower morphology predominated.

3.1.4. Reaction temperature

Since the polymerization process and free radical formation in the radical oxidation polymerization are considered exothermic reactions, removing heat from the synthesis environment (reducing the temperature of the synthesis environment) contributes to the development of the reaction and its optimal performance. Much research has been done on working out an appropriate temperature for aniline polymerization with high conversion (monomer to polymer) rates and appropriate crystallinity, most of which have reported low temperatures of about 3-5 ° C as the appropriate temperatures. In this study, the process of controlling aniline polymerization on the surface of the MWCNTs was performed at this temperature range, and tubular morphology was obtained.

3.1.5. Impact of morphology on the band gap

The band gap of the nanocomposites with two morphologies and their energy gap versus wavelengths are plotted in Figures 6a and 6b. As mentioned above, optimal dispersion and homogeneity of the nanotubes are achievable in the tubular morphology, and the ratio of the π-π bonds formed is more than the cauliflower morphology system [42]. Therefore, the band gap for transferring electrons from the valence bond to the conduction bond is lower—also, the transmission of wavelengths from blue to red covers a wider range in tubular morphology.

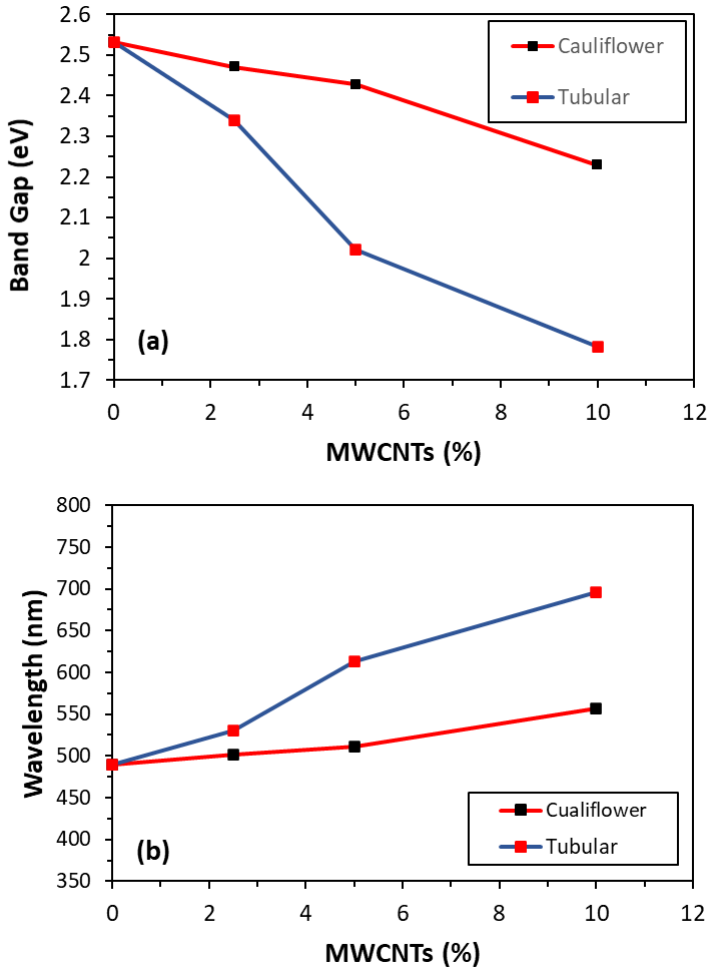

Figure 6. (a) The calculated band gaps and (b) the corresponding wavelengths for nanocomposites with two morphologies (Tubular and Cauliflower).

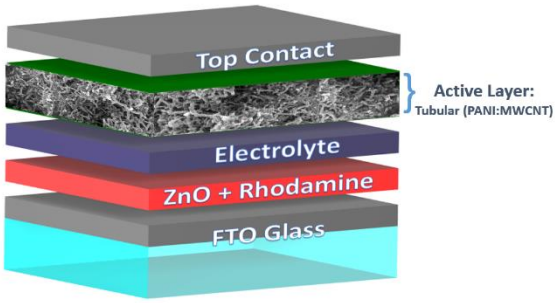

Figure 7. The schematic of the bulk heterojunction polymer solar cell structure with the tubular morphology PAni/MWCNT nanocomposite as the active layer.

3.2. PAni/MWCNT nanocomposite as an active layer of photovoltaic cell

The PAni/MWCNTs films were deposited over the FTO/ZnO glass substrate to prepare the polymer solar cell and used as an active layer. Figure 7 illustrates the scheme of the device structure.

3.2.1. The effect of MWCNT Wt. % on solar cell efficiency

To investigate the dependency of solar cell efficiency on the MWCNTs Wt. %, bulk heterojunction polymer solar cells were fabricated using PAni with a different percent of MWCNT (0%, 2.5%, 5%, and 10%). Figure 8 shows the J-V diagrams for these devices, and the results are abstracted in Table 2. It was observed that by increasing the amount of MWCNTs, the solar cell efficiency enhanced and the solar cells fabricated via the PAni/10 Wt.% MWCNTs as the active layer triggered the best device performance. As mentioned in the previous section, increasing the MWCNT Wt. % reduced the band gap and enhanced conductivity. As a result, the higher the amount of MWCNT, the easier it was to charge transfer, and ultimately, the efficiency of the solar cell increased. This is in agreement with the results obtained for the cauliflower morphology [37].

It is worth noting that by increasing the Wt. percent of MWCNTs, the increasing of efficiency rate gradually decreased, as shown in Figure 9. In addition to increasing the conductivity by adding MWCNTs, the mobility of the charge carriers and recombination was also enhanced. There was always a competition between the charge transfer and the recombination of charge carriers. In low amounts of MWCNTs, the charge transfer rate was higher than their recombination. Because there were enough paths to assist the charges to move away from each other, transferences were in the appropriate direction for collecting charges in the external circuit. When the amount of MWCNTs increased, the recombination rate also enhanced significantly (however, the separation rate was still higher than the recombination rate).

On the other hand, according to the results shown in Table 2, it can be seen that despite enhancing efficiency, increasing the amount of MWCNT led to a reduction of FF. One of the factors that greatly affected the FF was the recombination [43]. However, the addition of MWCNT had a greater impact on J_{SC} due to the creation of high percolation paths, and despite the reduction in FF, device performance was generally increased.

3.2.2. The dependency of solar cell efficiency on the morphology of the active layer

Table 3 presents the photovoltaic parameters of solar cells with the PAni/10% MWCNT nanocomposite as an active layer with tunable morphologies (cauliflower and tubular). The J_{sc} and V_{oc} of the cell with tubular morphology are increased significantly regarding a

Table 2. Photovoltaic properties of the PSCs based on PAni/MWCNTs tubular morphology with different weight percent of MWCNTs

MWCNTs Wt.%	V_{oc} (V)	J_{sc} (mA/cm²)	FF (%)	η (%)
0	0.0477	0.0101	0.024	0.000063
2.5	0.2497	0.0579	35	1.05
5	0.6575	0.1249	17	2.25
10	1.7329	0.0959	20.1	3.01

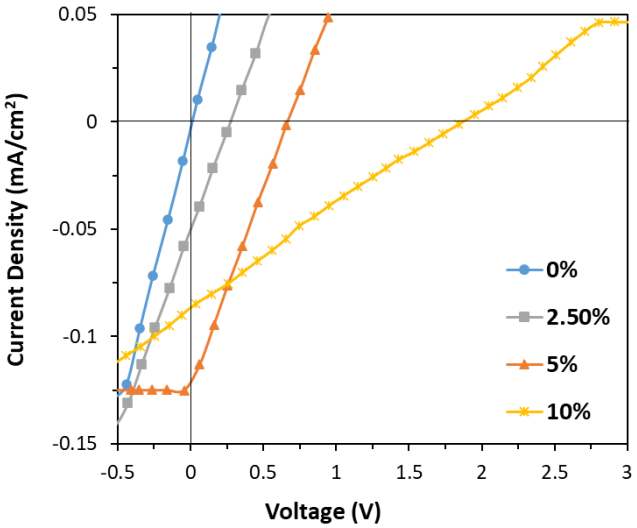

Figure 8. J-V diagrams of synthesized tubular nanocomposites with different weight percent of MWCNTs under the illumination of AM 1.5G, 100 mW/cm².

Table 3. Comparison between photovoltaic properties of PAni/10 Wt.% MWCNT nanocomposites with two morphologies

PSCs	V_{oc} (V)	J_{sc} (mA/cm²)	FF (%)	η (%)
Tubular morphology	1.7329	0.09592	20.1	3.01
Cauliflower morphology	0.5394	0.00111	0.34	1.04

device based on cauliflower morphology. Changing the active layer morphology from cauliflower to tubular form resulted in three times higher efficiency. The ratio of charge carrier recombination to separation depends strongly on the morphological tuning [44-47]. The recombination rate should reduce and the separation rate should increase to improve efficiency. Based on the experimental results obtained here, PAni/MWCNTs nanocomposites with the tubular morphology exhibited better photovoltaic behavior than nanocomposites with the cauliflower morphology. The reason for this behavior is the with the homogeneity of the components in tubular morphology, the photo-response of the nanocomposite improved. With the band gap reduction, the ability to charge transportation increased. In addition, enhancing FF leads to improved efficiency of

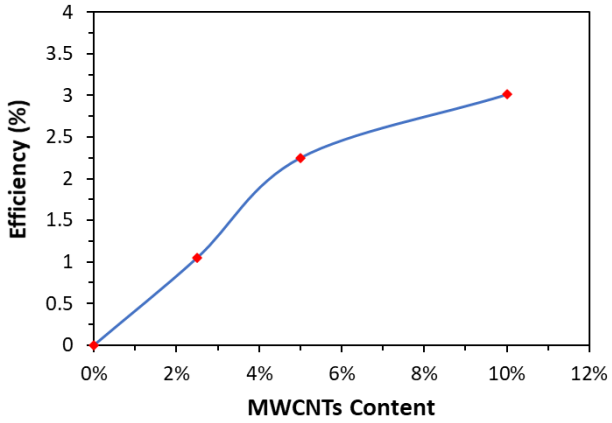

Figure 9. Efficiency versus MWCNTs weight percent behavior of PSCs based on PAni/MWCNTs with tubular morphology.

devices (about seventy times higher FF in Table 3 for tubular morphology). Besides, charge transfer in a crystalline structure is faster than in a structure with amorphous networks. The formed tubes with MWCNT core act as conductive bridges for electron transfer, and once the light is emitted at a special wavelength, the charges transfer more easily. Furthermore, as shown in Figure 5a, in tubular morphology, most of the nanotube surface is covered by polyaniline chains. This increases the interface area between the polymer matrix and the carbon nanotube, which acts as a tunnel for electron transfer so that the separation and transfer of charges can be promoted and the recombination rate can be diminished [48].

4. Conclusions

This study focused on synthesizing PAni/MWCNT nanocomposites with tunable morphologies and evaluating their application in polymer solar cells. The findings highlighted that tubular morphology outperformed cauliflower morphology in terms of conductivity, electron mobility, and band gap due to the efficient charge transfer pathways provided by tubular structures. Morphology control led to significant improvements in photovoltaic performance, including higher V_{OC}, J_{SC}, and FF, resulting in threefold higher efficiency. These enhancements were attributed to the better alignment and uniformity of MWCNTs, forming an effective percolation network. This work underscores the potential of morphology tuning in advancing organic solar cell performance and paves the way for further research and eventual commercialization of these devices.

Conflict of Interest

The author declares no conflict of interest.

References

1. 1. I. Burgués-Ceballos, et al. Towards industrialization of polymer solar cells: material processing for upscaling. *Journal of Materials Chemistry A*, **2014**, *2*, 17711.
2. R.A. Janssen and J. Nelson. Factors limiting device efficiency in organic photovoltaics. *Advanced Materials*, **2013**, *25*, 1847.
3. M. Glatthaar, et al. Efficiency limiting factors of organic bulk heterojunction solar cells identified by electrical impedance spectroscopy. *Solar energy materials and solar cells*, **2007**, *91*, 390.
4. Y. Li, et al. Flexible and semitransparent organic solar cells. *Advanced Energy Materials*, **2018**, *8*, 1701791.
5. S. Liu, et al. Enhanced efficiency of polymer solar cells by adding a high-mobility conjugated polymer. *Energy & Environmental Science*, **2015**, *8*, 1463.
6. S.R. Cowan, et al. Charge formation, recombination, and sweep-out dynamics in organic solar cells. *Advanced Functional Materials*, **2012**, *22*, 1116.
7. C. Groves. Developing understanding of organic photovoltaic devices: kinetic Monte Carlo models of geminate and non-geminate recombination, charge transport and charge extraction. *Energy & Environmental Science*, **2013**, *6*, 3202.
8. A. Baumann, et al. A new approach for probing the mobility and lifetime of photogenerated charge carriers in organic solar cells under real operating conditions. *Advanced materials*, **2012**, *24*, 4381.
9. K. Zhu, et al. Enhanced charge-collection efficiencies and light scattering in dye-sensitized solar cells using oriented TiO2 nanotubes arrays. *Nano letters*, **2007**, *7*, 69.
10. H. Lin, et al. Conducting polymer composite film incorporated with aligned carbon nanotubes for transparent, flexible and efficient supercapacitor. *Scientific reports*, **2013**, *3*, 1353.
11. K.-M. Lee, et al. Incorporating carbon nanotube in a low-temperature fabrication process for dye-sensitized TiO2 solar cells. *Solar Energy Materials and Solar Cells*, **2008**, *92*, 1628.
12. J. Arranz-Andrés and W.J. Blau. Enhanced device performance using different carbon nanotube types in polymer photovoltaic devices. *Carbon*, **2008**, *46*, 2067.
13. G. Keru, P.G. Ndungu, and V.O. Nyamori. A review on carbon nanotube/polymer composites for organic solar cells. *International Journal of Energy Research*, **2014**, *38*, 1635.
14. I. Jeon, et al. Single-Walled Carbon Nanotubes in Emerging Solar Cells: Synthesis and Electrode Applications. *Advanced Energy Materials*, **2019**, *9*, 1801312.
15. H.A. Alturaif, et al. Use of carbon nanotubes (CNTs) with polymers in solar cells. *Molecules*, **2014**, *19*, 17329.
16. S. Berson, et al. Elaboration of P3HT/CNT/PCBM composites for organic photovoltaic cells. *Advanced Functional Materials*, **2007**, *17*, 3363.
17. X.-L. Xie, Y.-W. Mai, and X.-P. Zhou. Dispersion and alignment of carbon nanotubes in polymer matrix: a review. *Materials science and engineering: R: Reports*, **2005**, *49*, 89.

18. Z. Jia, et al. Study on poly (methyl methacrylate)/carbon nanotube composites. *Materials Science and Engineering: A*, **1999**, *271*, 395.

19. F.C. Krebs. Fabrication and processing of polymer solar cells: A review of printing and coating techniques. *Solar energy materials and solar cells*, **2009**, *93*, 394.

20. A.C. Mayer, et al. Polymer-based solar cells. *Materials today*, **2007**, *10*, 28.

21. G. Li, R. Zhu, and Y. Yang. Polymer solar cells. *Nature photonics*, **2012**, *6*, 153.

22. M. Jørgensen, K. Norrman, and F.C. Krebs. Stability/degradation of polymer solar cells. *Solar energy materials and solar cells*, **2008**, *92*, 686.

23. H.-Y. Chen, et al. Polymer solar cells with enhanced open-circuit voltage and efficiency. *Nature photonics*, **2009**, *3*, 649.

24. S. Palaniappan and A. John. Polyaniline materials by emulsion polymerization pathway. *Progress in Polymer Science*, **2008**, *33*, 732.

25. C. Oueiny, S. Berlioz, and F.-X. Perrin. Carbon nanotube–polyaniline composites. *Progress in Polymer Science*, **2014**, *39*, 707.

26. S. Bhadra, et al. Progress in preparation, processing and applications of polyaniline. *Progress in polymer science*, **2009**, *34*, 783.

27. Y. Sun, S.R. Wilson, and D.I. Schuster. High dissolution and strong light emission of carbon nanotubes in aromatic amine solvents. *Journal of the American Chemical Society*, **2001**, *123*, 5348.

28. T.-M. Wu and Y.-W. Lin. Doped polyaniline/multi-walled carbon nanotube composites: Preparation, characterization and properties. *Polymer*, **2006**, *47*, 3576.

29. D.K. Kim, K. Wha Oh, and S.H. Kim. Synthesis of polyaniline/multiwall carbon nanotube composite via inverse emulsion polymerization. *Journal of Polymer Science Part B: Polymer Physics*, **2008**, *46*, 2255.

30. P. Jiménez, et al. Carbon nanotube effect on polyaniline morphology in water dispersible composites. *The Journal of Physical Chemistry B*, **2010**, *114*, 1579.

31. W. Ma, et al. Thermally stable, efficient polymer solar cells with nanoscale control of the interpenetrating network morphology. *Advanced Functional Materials*, **2005**, *15*, 1617.

32. Y. Huang, et al. Bulk heterojunction solar cells: morphology and performance relationships. *Chemical reviews*, **2014**, *114*, 7006.

33. S.N.K. Abad, et al. Growth mechanism and charge transport properties of hybrid Au/ZnO nanoprisms. *Journal of Alloys and Compounds*, **2019**, *777*, 1386.

34. F. Zhao, C. Wang, and X. Zhan. Morphology control in organic solar cells. *Advanced Energy Materials*, **2018**, *8*, 1703147.

35. B.C. Thompson and J.M. Fréchet. Polymer–fullerene composite solar cells. *Angewandte chemie international edition*, **2008**, *47*, 58.

36. Y. Liao, et al. Carbon nanotube/polyaniline composite nanofibers: facile synthesis and chemosensors. *Nano letters*, **2011**, *11*, 954.

37. R. Charekhah, et al. Bulk heterojunction solar cells based on polyaniline/multi wall carbon nanotube: from morphology control to cell efficiency. *Journal of Materials Science: Materials in Electronics*, **2019**, *30*, 26.

38. M. Campos and B. Bello Jr. Mechanism of conduction in doped polyaniline. *Journal of Physics D: Applied Physics*, **1997**, *30*, 1531.

39. S. Sinha, S. Bhadra, and D. Khastgir. Effect of dopant type on the properties of polyaniline. *Journal of Applied Polymer Science*, **2009**, *112*, 3135.

40. A. Imani and G. Farzi. VRH investigation of polyaniline–multiwalled carbon nanotube nanocomposite network. *Bulletin of Materials Science*, **2015**, *38*, 831.

41. A. Imani and G. Farzi. Low temperature process of electronic charge transport mechanism in PANi/MWCNT nanocomposites: tubular morphology. *Journal of Materials Science: Materials in Electronics*, **2017**, *28*, 10684.

42. S. Kondawar, M. Deshpande, and S. Agrawal. Transport properties of conductive polyaniline nanocomposites based on carbon nanotubes. *International Journal of Composite Materials*, **2012**, *2*, 32.

43. D. Bartesaghi, et al. Competition between recombination and extraction of free charges determines the fill factor of organic solar cells. *Nature communications*, **2015**, *6*, 7083.

44. D. Veldman, et al. Compositional and electric field dependence of the dissociation of charge transfer excitons in alternating polyfluorene copolymer/fullerene blends. *Journal of the American Chemical Society*, **2008**, *130*, 7721.

45. I.-W. Hwang, D. Moses, and A.J. Heeger. Photoinduced carrier generation in P3HT/PCBM bulk heterojunction materials. *The Journal of Physical Chemistry C*, **2008**, *112*, 4350.

46. T.M. Clarke, et al. Free energy control of charge photogeneration in polythiophene/fullerene solar cells: the influence of thermal annealing on P3HT/PCBM blends. *Advanced Functional Materials*, **2008**, *18*, 4029.

47. A. Gusain, R.M. Faria, and P.B. Miranda. Polymer Solar Cells—Interfacial Processes Related to Performance Issues. *Frontiers in chemistry*, **2019**, *7*, 61.

48. P. Peumans and S.R. Forrest. Separation of geminate charge-pairs at donor–acceptor interfaces in disordered solids. *Chemical Physics Letters*, **2004**, *398*, 27.